


**Experimental violations of Leggett-Garg inequalities on a quantum computer**Alessandro Santini<sup>1,\*</sup> and Vittorio Vitale<sup>1,2,†</sup><sup>1</sup>*SISSA, via Bonomea 265, 34136 Trieste, Italy*<sup>2</sup>*The Abdus Salam International Center for Theoretical Physics, Strada Costiera 11, 34151 Trieste, Italy* (Received 13 September 2021; revised 4 February 2022; accepted 9 March 2022; published 24 March 2022)

Leggett-Garg's inequalities predict sharp bounds for some classical correlation functions that address the quantum or classical nature of real-time evolutions. We experimentally observe the violations of these bounds on single- and multiqubit systems, in different settings, exploiting the IBM Quantum platform. In the multiqubit case, we introduce the Leggett-Garg-Bell's inequalities as an alternative to the previous ones. Measuring these correlation functions, we find quantum error mitigation to be essential to spot inequalities violations. Accessing only two qubit readouts, we assess Leggett-Garg-Bell's inequalities to emerge as the most efficient quantum coherence witnesses to be used for investigating quantum hardware, among those introduced. Our analysis highlights the limits of current quantum platforms, showing that the above-mentioned correlation functions deviate from theoretical prediction as the number of qubits and the depth of the circuit grow.

DOI: [10.1103/PhysRevA.105.032610](https://doi.org/10.1103/PhysRevA.105.032610)**I. INTRODUCTION**

As the effort to build fault-tolerant quantum computers increases, the need for efficient benchmarking and characterization of these devices becomes more and more apparent. Several studies have been realized in the direction of gauging current noisy intermediate-scale quantum (NISQ) devices [1]: some of them focus on the analysis of the entanglement behavior of these systems and ways of measuring it [2,3], while others propose new efficient entanglement detectors to be used in experiments [4–6]. In this work, we want to exploit Bell's-like inequalities in time, dubbed Leggett-Garg's inequalities (LGIs) [7,8], to test the quantum coherence of a quantum hardware. The availability of the open platform IBM Quantum [9] gives us the opportunity to carry out a rigorous study of its performance, highlighting, at same time, the power of LGIs as a witnesses of quantum coherence, applying them to real-world experiments.

A plethora of experimental tests of LGIs, and similar conditions, have already been performed on two-level systems [10–12] as well as more complicated experimental setups such as photonic systems, phosphorus impurities in silicon, superconducting devices, and nuclear magnetic resonances [13–19]. However, while numerical computation of LGIs to assess the quantum coherence of an open quantum systems has been carried out in the past [20,21], their investigation along the real-time dynamics of quantum hardware has rarely been considered as a topic of study [22,23]. As IBM Quantum becomes more popular [24–26] and its performance improves [27–29], we gauge it as the perfect remotely programmable playground for analyzing the prowess of LGIs in detecting quantum coherence [30–32].

Understanding the frontier between quantum and classical mechanics and how the latter arises from the former are open problems and vivid topics of study. Following the flood of studies about how macroscopic quantum coherence could be realized in the laboratory, Leggett and Garg wrote Bell's-like inequalities that test correlations of the same system measured at different times, in contrast with spatial Bell's inequalities that put constraints on the correlations of spatially separated systems [7,8]. The starting point of the LGIs is the definition of macrorealism. This is contained in a small set of principles which have been phrased as follows: (i) Macroscopic realism per se (MRPS): a macroscopic object with two or more, macroscopically distinct, available states is, at any given time, in a definite one of those states. (ii) Noninvasive measurability (NIM): it is possible, in principle, to determine in which of these states the system is, without any effect on the state itself or on the subsequent system dynamics. When one of these assumptions is not satisfied, one may assert that the system cannot be described by a macrorealistic theory, i.e., a theory which adheres to our intuition of how the macroscopic world should behave. Thus, assuming a quantum theory as the only alternative to a macrorealistic theory, LGIs can distinguish between classical and quantum systems.

In calculating LGIs, one considers consecutive measurements on a single system at different times and assumes NIM to hold. A heated argument which rises from this assumption is the so-called clumsiness loophole. This argument can be summarized as follows: Observing a LGI violation, a skeptical macrorealist might always appeal to hidden invasiveness of the measurements to explain the violations, since it is impossible to conclusively demonstrate that a physical measurement is, in fact, noninvasive [33]. The analogous loophole in Bell's inequalities is the communication loophole [34], which can be solved assuming that the measurements are sufficiently separated in space so that one measurement cannot influence the other. This is commonly known as the principle

\*asantini@sissa.it

†vvitale@sissa.it

of locality [35]. As an effort to go beyond the clumsiness loophole in LGIs, a hybrid version of the LGIs has been investigated [36–38]. These conditions, called Leggett-Garg-Bell’s inequalities (LGBIs), extend LGIs as both temporal and spatial Bell’s-like inequalities [36–39]. They assume the measurement of spatially separated parts of a system at different times so that the principle of NIM may be substituted by the principle of locality [35].

In general, most of the experimental tests of the LGIs conducted so far suffer from the clumsiness loophole [33] and it is still an open question whether loophole-free Leggett-Garg’s protocols can be constructed. In the only cases in which LGIs have been implemented on the IBM Quantum architecture [22,23], to the best of our knowledge, the authors circumvent the problem of NIM by use of an alternative witness. They introduce a condition that defines a “clumsy macrorealism” which embodies the possibility of modifications of the state of the system after a measurement and discuss its properties in several settings.

Also, in the case of LGBIs, for the principle of locality to hold, one may observe that the parts of the system which are measured should be infinitely distant or distant enough according to the Lieb-Robinson bound [40], a condition which may not be satisfied in the settings we are interested in.

In this work, we will not discuss these technicalities in detail; nevertheless, we believe our work may stimulate the search for generalizations of LGIs and LGBIs where the NIM-locality assumption can be relaxed. For a more detailed treatment of the loopholes of both LGIs and LGBIs, we encourage the reader to consult Refs. [23,41] and references therein.

Evidently, quantum hardware may benefit from quantum coherence witnesses, such as LGIs and LGBIs, acting as a benchmark of their proper functionality. At the same time, investigating theoretical bounds of correlation functions on experimental setups is quite interesting on its own, from a fundamental standpoint. With this in mind, we first introduce LGIs and LGBIs; then, we discuss the prototypical example of a single qubit (spin-1/2), evolving under a unitary dynamics, comparing the experimental results against the theoretical ones. We measure the LGIs for one of the IBM Quantum transmons, which plays the role of a quantum qubit, evolving with its own dynamics, experimentally showing the effects of decoherence on the hardware. This allows us to roughly estimate the value of the coherence time  $\langle T_2 \rangle$  of the transmon, in agreement with the nominal value for the processor used and the effective dynamics which describes it. Moreover, we investigate multiqubit systems, calculating LGIs and LGBIs in different settings. We observe LGIs and LGBIs violations in several experimental setups, addressing the quantum coherence of the hardware in the timescales investigated. Finally, we apply LGBIs to a many-body example, namely, the transverse field Ising model, to show that the performance of the hardware worsens with an increasing depth of the circuit. This result allows us to elaborate on the quantum coherence of IBM Quantum processors in the case of multiqubit computations and draw our conclusions. Error mitigation is exploited during this work to improve the performance of the readouts of the IBM Quantum processors. We observe that such procedure is essential to witness most of the inequalities violations we

address, thus showing the limits of the hardware and the power of LGIs and LGBIs alike.

## II. LEGGETT-GARG’S INEQUALITIES

Leggett-Garg’s inequalities predict thresholds for classical correlation functions which can be violated if the system behaves according to quantum mechanics. Their definition is based on the concept of macrorealism that is encoded in a set of assumptions which a classical system must stick to [8,41]. Based on the assumptions introduced above, Leggett and Garg derived Bell’s-like inequalities that any system behaving “classically” should obey. Violations of these inequalities provide evidence of quantum behavior of a system if it is accepted that the alternative to classical theories is quantum mechanics. In Appendix A, we present a detailed derivation of the LGIs, according to [41], for the sake of completeness. Here we introduce the basic details and show the inequalities we will use for the remainder of the work.

Let us define a classical dichotomic variable  $Q$  which can assume values  $+1$  or  $-1$ :  $Q(t_i) = Q_i$  stands for the measurement value of the observable at time  $t_i$ . We denote with  $P_i(Q_i)$  the probability of obtaining the result  $Q_i$ . The correlation function  $C_{ij}$  is written as

$$C_{ij} = \sum_{Q_i, Q_j = \pm 1} Q_i Q_j P_{ij}(Q_i, Q_j), \quad (1)$$

where the subscripts of  $P$  remind us of the times at which the measurements are performed. Assuming the principle introduced before to hold, one can prove that

$$\begin{aligned} K_3 &= C_{12} + C_{23} - C_{13}, & -3 \leq K_3 \leq 1; \\ K'_3 &= -C_{12} - C_{23} - C_{13}, & -3 \leq K'_3 \leq 1; \\ K_3^{\text{perm}} &= -C_{12} + C_{23} + C_{13}, & -3 \leq K_3^{\text{perm}} \leq 1. \end{aligned} \quad (2)$$

These are all the conditions of the possible different correlations functions one can derive at third order, namely, performing three measurements in time,  $t_1 < t_2 < t_3$ .

Even though LGIs are not necessary conditions to assess the quantum coherence of the time evolution [42,43], they have been successfully utilized to address this problem in the study of open quantum systems [20,21].

## III. LEGGETT-GARG-BELL’S INEQUALITIES

Leggett-Garg’s inequalities can be computed on any kind of systems as the only prerequisite is the definition of a dichotomic variable. Taking into account a large ensemble of qubits, it is possible to exploit them considering a global variable, e.g., total angular momentum or spin, as done in Refs. [44,45]. From an experimental point of view, it may lead to bigger errors in the computation as it implies the readout of all the qubits. Remarkably, it is possible to take into account different inequalities that circumvent this problem. The rationale behind this extension is to substitute the NIM postulate with the one of locality as anticipated before. In this framework, measurements are made at different times and at distinct locations, so that locality can be invoked to justify noninvasiveness. The analytical derivation of the inequalities is equivalent to the one of the LGIs where the second

measurement is performed on a different location. Here we define the correlation function  $C_{ij}^{AB}$  as

$$C_{ij}^{AB} = \sum_{Q_i^A, Q_j^B = \pm 1} Q_i^A Q_j^B P_{ij}^{AB}(Q_i^A, Q_j^B), \quad (3)$$

where the subscripts  $i, j$  denote the times when the measurements are performed and the superscripts  $A, B$  are two spatially separated locations. Considering macroscopic realism and ‘‘Bell-macroscopic locality,’’ one gets [38,39]

$$\begin{aligned} T_3 &= C_{12}^{AB} + C_{23}^{AB} - C_{13}^{AB}, & -3 \leq T_3 \leq 1; \\ T'_3 &= -C_{12}^{AB} - C_{23}^{AB} - C_{13}^{AB}, & -3 \leq T'_3 \leq 1; \\ T_3^{\text{perm}} &= -C_{12}^{AB} + C_{23}^{AB} + C_{13}^{AB}, & -3 \leq T_3^{\text{perm}} \leq 1, \end{aligned} \quad (4)$$

at third order, i.e., considering three time instants.

The introduction of the LGB’s correlation functions  $T$  will be very useful for us in the context of gauging IBM Quantum. In fact, since they involve the measurement of only two qubits but intrinsically take into account the spatial degrees of freedom of the system, they might be a valid alternative to LGIs on multiqubit systems.

#### IV. SINGLE-QUBIT EXPERIMENTS

##### A. Time evolution of a single qubit

The starting point of the investigation of LGIs would naturally be the canonical example of a qubit evolving under the Hamiltonian

$$H = \frac{\Gamma_x \sigma_x}{2}, \quad (5)$$

where  $\Gamma_x$  is the qubit frequency (we set  $\hbar = 1$ ). It can be used both as an introduction to how LGIs work and can be interpreted, as well, as a first benchmark of the IBM Quantum hardware. The analytical calculation of the LGIs for a two-level system is straightforward and proceeds as follows. First, we choose  $\hat{Q} = \sigma_z$  as the dichotomic operator taking values  $\pm 1$  if the  $z$  component of the spin of the qubit is up or down. Second, since the evolution operator,

$$U(t) = e^{-i \frac{\Gamma_x \sigma_x}{2} t}, \quad (6)$$

is a simple rotation around the  $x$  axis, the correlation  $C_{ij}$  takes the analytical expression [41,46]

$$C_{ij} = \cos \Gamma_x (t_j - t_i). \quad (7)$$

If we set  $t_3 - t_2 = t_2 - t_1 = \tau$ , we can express the functions  $K_3, K'_3, K_3^{\text{perm}}$  in terms of the time difference between the two measurements:

$$\begin{aligned} K_3 &= 2 \cos \Gamma_x \tau - \cos 2\Gamma_x \tau, \\ K'_3 &= -2 \cos \Gamma_x \tau - \cos 2\Gamma_x \tau, \\ K_3^{\text{perm}} &= \cos 2\Gamma_x \tau. \end{aligned} \quad (8)$$

These functions oscillate in time and violate the inequalities only for certain values of  $\tau$ . The quantities in Eq. (8) are plotted in Fig. 1 as continuous curves. As shown in Fig. 1 and observed in Ref. [47],  $K_3$  and  $K'_3$  appear to be complementary: one is violated when the other is not, and vice versa. This

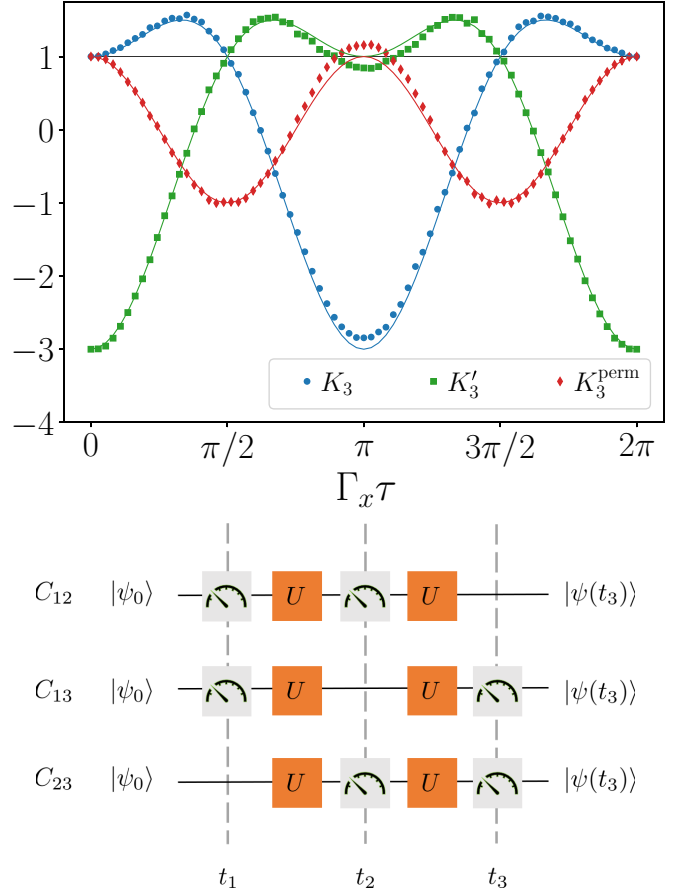


FIG. 1. Top: LGIs as a function of the time difference between two subsequent measurements (circuit depth 7). The curves show  $K_3, K'_3,$  and  $K_3^{\text{perm}}$ , according to Eq. (8). The violation threshold is marked by the solid black line. Markers are experimental results; solid lines are theoretical predictions. The error bars are not visible as the statistical error is about  $10^{-2}$ . Bottom: Diagram of the evolution and the measurement scheme.

complementary behavior allows a detection of the nonclassical properties of the two-level system over the full parameter range.

It can be seen that this is just a particular case due to the specific choice of the Hamiltonian and the dichotomic variable. Hence one should not be misled that third-order LGIs can provide a comprehensive picture of the physics of the system. However, as already pointed out, the comparison between the theoretical and experimental calculation of LGIs may be informative of the performance of the hardware and the experimental setup that is used.

The evolution of the system considered in this section is straightforwardly implemented in IBM Quantum. We consider  $N_\tau = 75$  values for  $\tau \in [0, 2\pi/\Gamma_x]$  and evaluate  $C_{ij}$ , in particular,

$$\begin{aligned} C_{12}(\tau) &= \langle \sigma^z(0) \sigma^z(\tau) \rangle, \\ C_{13}(\tau) &= \langle \sigma^z(0) \sigma^z(2\tau) \rangle, \\ C_{23}(\tau) &= \langle \sigma^z(\tau) \sigma^z(2\tau) \rangle, \end{aligned} \quad (9)$$

measuring the spin along the  $z$  axis at the two appropriate time instants, as shown in the bottom panel of Fig. 1. We

repeat each evolution, together with the needed measurements,  $n_{\text{shots}} = 2^{13}$  times. In the upper panel, we show the results of the experiment performed on the IBM Quantum open-access hardware `ibmq_manila` (markers) and the analytical predictions according to Eq. (9) (solid lines). Error bars are not visible as the error on the measurement outcomes should be estimated of the order of  $1/\sqrt{n_{\text{shots}}} \approx 10^{-2}$ .

From Fig. 1 is evident that the experimental results deviate from Eq. (8) around  $\Gamma_x \tau \sim \pi$  even though the qualitative picture is the same. Remarkably, while the results are not perfectly in agreement with the theoretical ones, we see that the LGIs threshold is always violated, witnessing that the interaction with the environment does not spoil the quantum dynamics. We seize this opportunity to mention that all the shown experimental results are obtained performing error mitigation. A detailed explanation of how it works and its huge influence on the outcomes is given in Appendix B.

### B. Transmon qubit

An interesting case study, in relation with IBM Quantum, is analyzing the evolution of one of the qubits of the quantum hardware when it is left untouched by the quantum circuit. The processors provided by IBM Quantum are constituted by transmons which can be modeled, for our purposes, as a two-level system described by the Hamiltonian

$$H^{\text{eff}} = -\frac{\hbar\Omega}{2}\sigma^z. \quad (10)$$

It is possible to measure the LGIs on this system in the following way. Since one is interested in the dynamics of the transmon according to  $H^{\text{eff}}$ , one can force the hardware to evolve acting on an ancilla qubit with identity gates. In this way, the transmon we are interested in would not be touched by the quantum gates and would evolve under its intrinsic “physical” Hamiltonian  $H^{\text{eff}}$ . In  $H^{\text{eff}}$ ,  $\Omega \simeq 4.971$  GHz is the nominal frequency of the qubit used for the experiment [9]. Since the default initial state of the processors is  $|0\rangle$ , the qubit is rotated in the state  $|+\rangle = \frac{1}{\sqrt{2}}(|0\rangle + |1\rangle)$  by use of a Hadamard gate at the initial time. Then the evolution is executed. The qubit rotates in the same fashion discussed in relation to Fig. 1, with its own intrinsic frequency  $\Omega$ . In Fig. 2, we plot the LG’s correlation functions  $K$  as a function of time. We observe that the threshold 1 is violated multiple times, for  $t < 30 \mu\text{s}$ . For long evolution times, the dynamics is damped, witnessing the loss of coherence in the system. The average coherence time estimated for the quantum hardware that we used (`ibmq_manila`), according to IBM, is  $\langle T_2 \rangle \sim 55 \mu\text{s}$ . We observe that assuming the theoretical behavior to hold, i.e., without any damping (dashed lines),  $K_3$  should have exceeded the threshold periodically. However, the experimental results do not violate the LGIs where one would have expected it to theoretically ( $t \sim 45 \mu\text{s}$ ). This is quite in agreement with the coherence time  $\langle T_2 \rangle \sim 55 \mu\text{s}$  predicted by IBM Quantum. Here we point out that the nominal coherence time average  $\langle T_2 \rangle$  is estimated at each recalibration of the processors. The value we write here is the one reported at the time the experiment was performed.

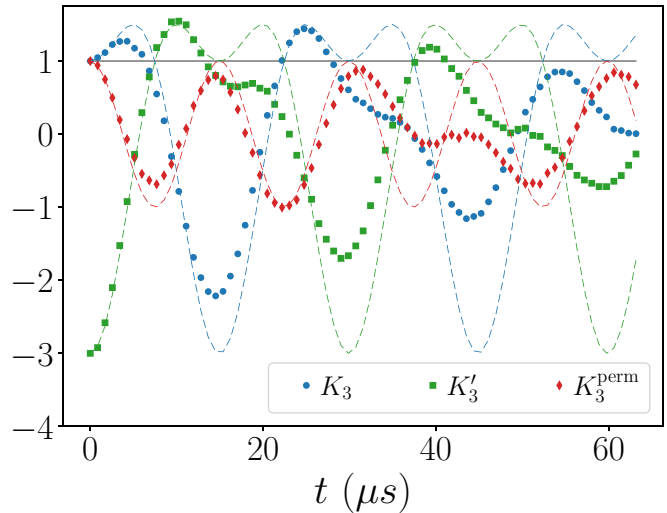


FIG. 2. LGIs as a function of the time difference between two subsequent measurements calculated on the transmon qubit evolution. The dashed curves are the theoretical predictions according to Eq. (8); the markers are the experimental results (statistical error is less than the size of the markers). A violation does not occur after  $t \sim 45 \mu\text{s}$  in the experimental data, witnessing the loss of coherence of the system. This is compatible with IBM Quantum estimation (at the time of the experiment) of the coherence time for the used system (`ibmq_manila`):  $\langle T_2 \rangle = 55 \mu\text{s}$ . The error bars are not visible as the statistical error is about  $10^{-2}$ .

## V. MULTIQUBIT EXPERIMENTS

The ultimate goal of quantum computation is realizing a scalable and fault-tolerant quantum computer, which allows the usage of a large ensemble of qubits, taming the errors accumulating during the computation. For this reason, we want to investigate the behavior of the inequalities we have introduced in multiqubit systems, to highlight their usefulness and efficiency. In multiqubit systems, the LGIs would require a dichotomic variable which is defined on the entire ensemble [45]. For instance, one could choose the total spin along the  $z$  axis,  $S^z = \sum_i \sigma_i^z$ . With increasing system size, however, not only do the sources of error during the computation accumulate, but also the ones due to readouts, when measuring the whole ensemble of qubits. We point out that the readout error is a huge constraint for IBM Quantum and error mitigation complexity scales exponentially with the system size. For this reason, one would like to narrow the number of qubits to be measured to the smallest possible amount. With this in mind, we will exploit LGIs which, by definition, take into account both temporal and spatial correlations in the system and only require two readouts. We will compare the LGIs with the LGIs, which can be defined both by performing measurements on a single qubit and on all the qubits, and discuss their limitations.

### A. Noninteracting qubits

Let us start by considering a two-qubit system. We investigate LGIs calculated performing measurements on a single qubit (LGIs single qubit), LGIs where the dichotomic variable is a global one (LGIs multiqubit), i.e., measuring all

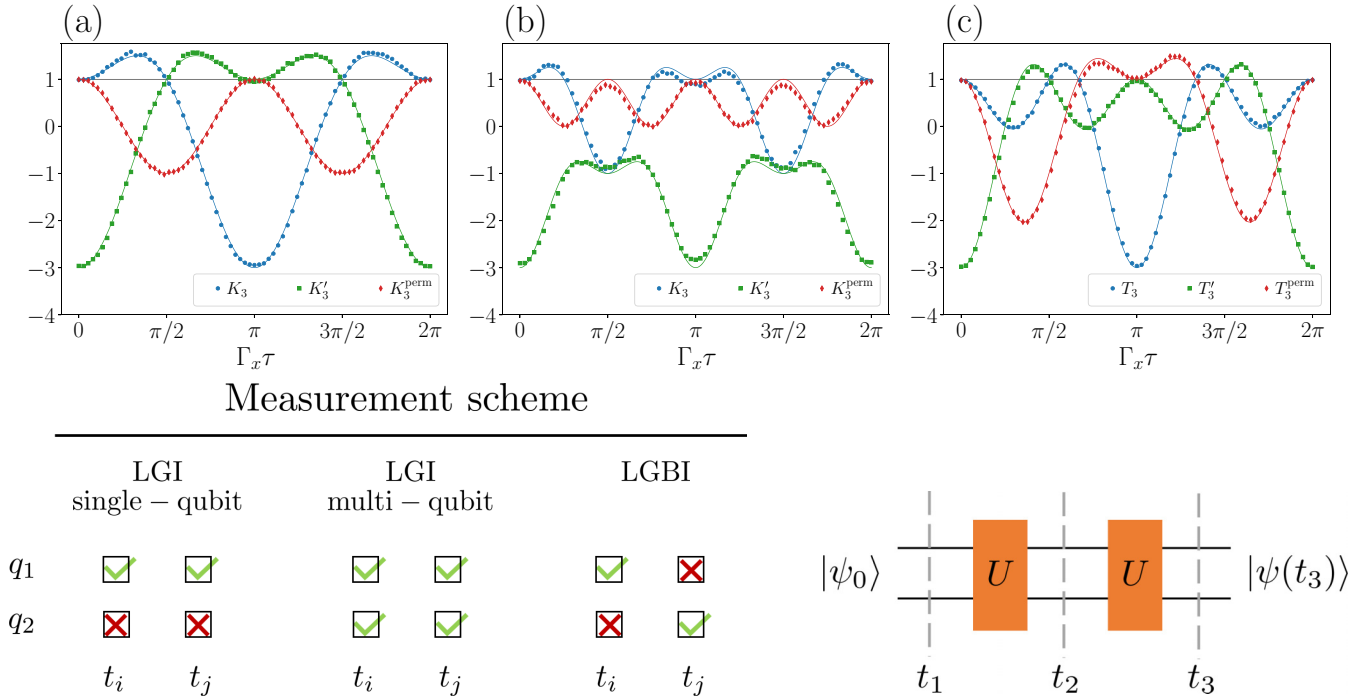


FIG. 3. LGBIs and LGIs on a two-qubit system. Markers are experimental results (statistical error is less than the size of the markers); solid lines are numerical predictions obtained with exact diagonalization. (a) LGIs calculated on a single qubit (circuit depth 11); (b) LGIs considering the total spin of the system (circuit depth 11); (c) LGBIs (circuit depth 10). The horizontal line marks the threshold of the inequalities. Bottom: Measurement scheme for calculating a LGI and LGBI and diagram of the evolution. Red crosses in the measurement scheme label qubits which are not measured at times  $t_i$  and  $t_j$ ; green check marks denote the qubits that are measured.

the qubits, and LGBIs where two readouts on two different qubits are realized. We examine the dynamics of two qubits, initially entangled, evolving independently according to the Hamiltonian

$$H = \sum_{i=1}^N \frac{\Gamma_i}{2} \sigma_i^x, \tag{11}$$

and measured at times  $t_1, t_2, t_3$ ; here,  $\Gamma_i = \Gamma_x \forall i$ . As before, we will assume  $t_2 - t_1 = t_3 - t_2 = \tau$  and plot the results as

$$C_{ij}(t_i, t_j) = \langle \hat{Q}(t_i) \hat{Q}(t_j) \rangle = \sum_{n,m} q_n q_m \text{Tr}[\Pi_m U(t_j, t_i) \Pi_n U(t_i, 0) \rho_0 U^\dagger(t_i, 0) \Pi_n U^\dagger(t_j, t_i) \Pi_m]. \tag{13}$$

Here,  $q_n$  are the possible values of the dichotomic observable  $\hat{Q}$ ,  $\Pi_n$  are the corresponding projection operators,  $U(t_j, t_i) = e^{-iHt}$  is the evolution operator, and  $\rho_0$  is the density matrix of the system at time  $t = 0$ . This expression can be easily calculated analytically in the case of noninteracting Hamiltonians [45] and numerically in the case of interacting ones. A sketch of the evolution and of the measurement scheme is depicted in the bottom panels of Fig. 3. Each upper panel plot corresponds to a different setup described in the lower left plot, “Measurement scheme”: the rows  $q_1, q_2$  correspond to the two qubits of the system and the columns  $t_i, t_j$  denote the times at which measurements are performed. We mark the

a function of the time difference  $\tau$ . The initial state of the system is a Bell state,

$$|\psi\rangle = \frac{1}{\sqrt{2}}(|00\rangle + |11\rangle), \tag{12}$$

obtained by use of a Hadamard gate and a CNOT. For each setup that we have introduced above (LGIs single qubit, LGIs multiqubit, LGBIs), we take  $N_\tau = 75$  values for  $\tau \in [0, 2\pi/\Gamma_x]$  and repeat each simulation  $n_{\text{shots}} = 2^{13}$  times on ibmq\_manila. The continuous lines in Fig. 3 are obtained by calculating the correlation function exactly according to

square box with a red cross if a qubit is left untouched by the measurements at a given time; we check it with green check marks if the qubit is measured instead.

In Fig. 3(a), we perform two measurements, for each choice of  $\tau$ , on the same qubit (LGIs single qubit). We choose as dichotomic variable  $\sigma_1^z$  (considering  $\sigma_2^z$  would be analogous) and calculate the LGIs. Evidently, the result is equivalent to the one in Fig. 1. We ascribe this behavior to the fact that single-qubit LGIs are measuring the coherence of the single qubit and they cannot provide information on the full system, even if the qubits are entangled at the beginning of the evolution. In Fig. 3(b), we calculate the LGIs choosing

a dichotomic observable defined on the whole system, namely,  $\hat{Q} = 2|\sum_i \sigma_i^z| - 1 = \sigma_1^z \sigma_2^z$  (LGIs multiqubit). Evidently, a violation of the LGIs occurs. This allows us to affirm that LGIs can be used to detect the quantum coherence during the evolution in the time interval that is considered. Since we are using a global observable, we are confident that the information provided concerns the whole system. The bottleneck of multiqubit LGIs is the required number of single-qubit readouts. Since it scales with the size of the system and error mitigation is mandatory, as discussed in Appendix B, it is not affordable for large system sizes.

Finally, in Fig. 3(c), we calculate the LGBIs measuring  $\sigma_1^z$  and  $\sigma_2^z$ . We observe that LGBIs are also able to detect the quantum coherence of the evolution. In this experimental setup, the violation is much stronger than in the case of LGIs multiqubit; however, one cannot assert with generality that LGBIs exhibit stronger violations with respect to LGIs in all cases.

Let us comment that LGBIs can detect the quantum coherence with only two single-qubit readouts instead of measuring an observable defined on the whole system. Evidently, it would be interesting to expand the investigation to larger systems. For this reason, in the following, we will focus on LGBIs to observe if they are able to witness the quantum coherence of the system also in a many-body scenario.

### B. Interacting qubits

Having understood that the family of inequalities we have introduced can be successfully exploited to witness the quantum coherence of a quantum evolution, from now on the focus of the study will be the performance of the hardware used to investigate exploiting LGBIs. In particular, we will discuss an interacting quantum many-body system to elaborate on the performances of IBM Quantum in a physically intriguing setup.

Simulating interacting systems on quantum computers is well known to be a famously daunting task and bound by very small coherence times [48,49]. In this respect, we decided to consider an interacting evolution where the interaction contribution is a slight perturbation over a noninteracting dynamics.

Here we investigate a system of  $N = 5$  qubits, initially entangled in a Greenberger–Horne–Zeilinger (GHZ) state  $(|00000\rangle + |11111\rangle)/\sqrt{2}$ , to be reproduced on `ibmq_manila`,

TABLE I. Circuit depth of the circuits related to Fig. 4 for different values of the number of Trotter steps. In columns  $C_{12}$  and  $C_{13}$ ,  $C_{23}$ , we write the circuit depths related to the circuits used to estimate  $C_{12}$  and  $C_{13}$ ,  $C_{23}$ , respectively.

Trotter steps	$C_{12}$ (depth)	$C_{13}, C_{23}$ (depth)
$k = 1$	18	29
$k = 2$	29	51
$k = 3$	40	73
$k = 4$	51	95
$k = 5$	62	117

during a transverse-field-Ising-chain-like (TFIC) evolution described by the Hamiltonian

$$H = -J \sum_{i=1}^{N-1} \sigma_i^z \sigma_{i+1}^z - \sum_{i=1}^N \Gamma_i \sigma_i^x; \quad (14)$$

$N = 5$  is the maximum number of qubits available in `ibmq_manila`. We measure  $\sigma_1^z$  and  $\sigma_2^z$  to calculate the LGBIs. We consider  $J = 0.1$  and  $\Gamma_i = 1$  for  $i = 1, \dots, 4$ ,  $\Gamma_5 = 2$ . The choice of the parameters is made in order to have a violation of the inequalities for  $\Gamma_1 \tau < 1$  (see Appendix C for more details).

In order to implement the evolution on the quantum hardware, exploiting the fact that the interaction is nearest neighbors, we split the Hamiltonian in  $H_{\text{even}} = \sum_{i \text{ even}} \sigma_i^z \sigma_{i+1}^z$  and  $H_{\text{odd}} = \sum_{i \text{ odd}} \sigma_i^z \sigma_{i+1}^z$ , then we approximate  $U(dt) \approx e^{-iH_{\text{even}} dt} e^{-iH_{\text{odd}} dt}$ . To investigate the behavior of IBM Quantum for different circuit depths, we set the number of applications of  $U(dt)$  at  $k = 1, 2, 3, 4, 5$  with  $dt = \tau/k$ .

In Fig. 4, the experimental outcomes of  $T_3$ ,  $T'_3$ ,  $T_3^{\text{perm}}$  are shown together with the theoretical predictions. In each panel, we plot several curves for different values of the number of Trotter steps, as a function of time. In Table I, we write the circuits depths for the different implementations considered. While the agreement between numerical and experimental simulations should improve upon increasing the number of steps in the Trotterization, as the approximation of the evolution is more accurate, we observe that the experimental results deviate more and more from the theoretical prediction with increasing  $k$ . We believe this is due to the errors accumulating during the computation, which grow with the number

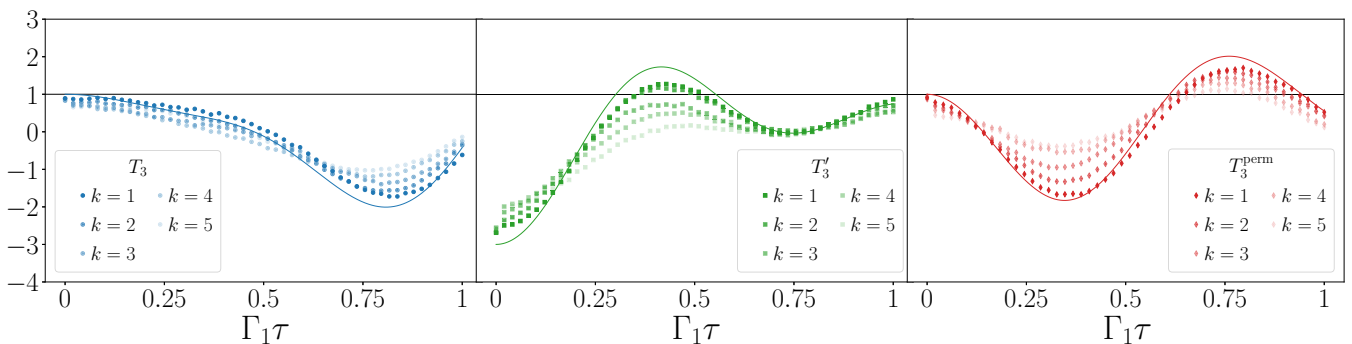


FIG. 4. Transverse field Ising chain,  $J = 0.1$   $\Gamma_i = 1$ ,  $i = 1, \dots, 4$ ,  $\Gamma_5 = 2$ . Markers are experimental results (statistical error is less than the size of the markers); the curves are obtained according to Eq. (13). We observe an experimental violation of the LGBIs.

of gates implemented in the circuit. Furthermore, we observe that while the agreement between experiments and numerical simulations is not perfect, the qualitative behavior is somehow reproduced and it is possible to observe a violation of the inequalities both in  $T_3'$  and  $T_3^{\text{perm}}$  for several values of circuit depths. This could be used to estimate the coherence time of the many-body system since, considering longer simulations, one could expect that no other violation of the inequalities occurs as the number of applied gates increases.

## VI. CONCLUSIONS

With the advent of modern technologies, the study of entanglement and quantum coherence of physical systems is crossing the boundaries of purely theoretical interest and is starting to intertwine with the practical investigation of now available quantum platforms. For this reason, reliable entanglement detectors and entanglement witnesses are becoming more and more important. In this work, we have decided to exploit IBM Quantum processors to investigate a class of well-known quantum coherence witnesses. We have introduced Leggett-Garg's inequalities (LGIs) and Leggett-Garg-Bell's inequalities (LGBIs) and measured their outcomes in different physical setups, taking advantage of the versatile programmable nature of IBM Quantum.

We have shown experimental violations of the LGIs and LGBIs in single- and multiqubit systems. We have observed that by investigating reasonable timescales, the LGIs are in agreement with theoretical results in noninteracting systems, witnessing that the IBM Quantum processor used here (ibmq\_manila) is robust against decoherence at early times. Furthermore, we have explicitly investigated the coherence of one of the transmons constituting the ibmq\_manila processor. We let it evolve under its own dynamics, according to the effective transmon Hamiltonian, and observed that LGIs violations do occur up to a characteristic time which is compatible with the nominal coherence time of the system,  $\langle T_2 \rangle$ . The nominal value of  $\langle T_2 \rangle$  considered here is the one which has been estimated at the time of the experiment.

To further deepen the investigation of the Leggett-Garg's-like inequalities, we have considered two-qubit systems where the qubits, initially entangled in a Bell's state, evolve independently. We have made a comparison among LGIs using a single-qubit dichotomic variable, LGIs using a global observable, and LGBIs. We have shown that LGBIs provide the same violation of the threshold as LGIs in the investigated time range, requiring only two readouts. As a consequence, one can focus on the calculation of LGBIs for studying multiqubit systems.

Furthermore, we have elaborated on the necessity of error mitigation for the observation of the inequalities violations in a wide range of the time interval. Error mitigation complexity scales exponentially with the system size and quickly becomes unfeasible for the estimation of LGIs using a multiqubit observable. Then, LGBIs also show the merit of requiring only two measurements, whatever the size of the system, such that error mitigation is always possible after the experiments.

To apply the condition we have introduced to a relevant physical case and to benchmark the IBM Quantum platform, we discussed a quantum many-body problem where inter-

action is added as a small perturbation on a noninteracting dynamics. In this simple case, where the value of the parameters is fine tuned, we observed that experimental results violate the threshold, but deviate from the curves predicted by the analytical results. Furthermore, we showed that quantum coherence is lost, increasing the number of gates of the system.

In conclusion, our results both show the experimental observation on a quantum computer of violations of Leggett-Garg's type inequalities and provide evidence of the usefulness of these quantum witnesses in the context of NISQ devices. The results also suggest that by increasing the circuit depth, even LGBIs, which emerge as the most efficient witness among those introduced, rapidly depart from the theoretical prediction and may fail in detecting quantum coherence since the gates errors accumulate.

As we have observed that Leggett-Garg's-type inequalities can be successfully used to discriminate against classical or quantum evolution, one would be interested in checking their behavior with larger system sizes and more complex quantum circuits. It could also be interesting to investigate particular topologies, not currently available in IBM Quantum, which allow one to connect an ancilla to all the qubits performing a given computation, in order to assess if ancilla-based methods may be beneficial in this framework.

The data that support the plots within this paper and other findings of this study are available from the authors upon request.

## ACKNOWLEDGMENTS

We are grateful to M. Dalmonte, G. Santoro, and A. Galvani for valuable discussions. We acknowledge the use of IBM Quantum services for this work [9]. The views expressed are those of the authors, and do not reflect the official policy or position of IBM or the IBM Quantum team. V.V. acknowledges support by the ERC under Grant No. 758329 (AGEnTh), and has received funding from the European Union's Horizon 2020 research and innovation programme under Grant Agreement No. 817482 (Pasquans). The authors acknowledge that their research has been conducted within the framework of the Trieste Institute for Theoretical Quantum Technologies (TQT).

V.V. set the theoretical framework. A.S. performed the simulations and the experiments on IBM Quantum. All authors discussed and contributed in writing the manuscript.

The authors have no potential financial or nonfinancial conflicts of interest.

## APPENDIX A: DERIVATION OF LGI

Let us derive the Leggett-Garg's inequalities in Eq. (8) explicitly. Derivation of LGBI is analogous where Bell locality plays the role of NIM.

Let us start with the definition of a classical dichotomic variable  $Q$ . It must take two values  $Q = \pm 1$ , but it is not necessarily associated to a dichotomic operator [45]. We use  $Q(t_i) = Q_i$  to denote the measurement value of the observable at time  $t_i$ . Finally, we label the probability of obtaining the result  $Q_i$  at time  $t_i$  as  $P_i(Q_i)$ . Therefore, the correlation function

$C_{ij}$  can be defined as follows:

$$C_{ij} = \sum_{Q_i, Q_j = \pm 1} Q_i Q_j P_{ij}(Q_i, Q_j), \quad (\text{A1})$$

where the subscripts of  $P$  are used to explicitly remind the reader of the times at which the measurements were performed. The assumption of macrorealism per se guarantees that  $P_{ij}$  can be obtained as the marginal probability of  $P_{ijk}(Q_i, Q_j, Q_k)$ ,

$$P_{ij} = \sum_{Q_k: k \neq i, j} P_{ijk}(Q_i, Q_j, Q_k). \quad (\text{A2})$$

$$\begin{aligned} C_{12} &= P(+, +, +) + P(+, +, -) + P(-, -, +) + P(-, -, -) - P(+, -, +) - P(+, -, -) - P(-, +, +) - P(-, +, -), \\ C_{13} &= P(+, +, +) + P(+, -, +) + P(-, +, -) + P(-, -, -) - P(+, +, -) - P(+, -, -) - P(-, +, +) - P(-, -, +), \\ C_{23} &= P(+, +, +) + P(-, +, +) + P(+, -, -) + P(-, -, -) - P(+, +, -) - P(-, +, +) - P(+, -, +) - P(-, -, +), \end{aligned} \quad (\text{A4})$$

where we have used  $P(\pm, \pm, \pm) = P(\pm 1, \pm 1, \pm 1)$ .

Exploiting the completeness relation  $\sum_{Q_i, Q_j, Q_k} P(Q_i, Q_j, Q_k) = 1$ , we obtain  $K_3 = C_{12} + C_{23} - C_{13}$ :

$$K_3 = 1 - 4[P(+, -, +) + P(-, +, -)]. \quad (\text{A5})$$

The upper bound of  $K_3$  is given by  $P(+, -, +) = P(-, +, -) = 0$ , which is  $K_3 = 1$ ; the lower bound, instead, is given by  $P(+, -, +) + P(-, +, -) = 1$ , and hence  $K_3 \geq -3$ . Besides the above inequality, that is,

$$-3 \leq K_3 \leq 1, \quad (\text{A6})$$

other inequalities exist, which can be found in the literature.

Various symmetry properties may be used to derive further constraints on the correlations. First, we can redefine the

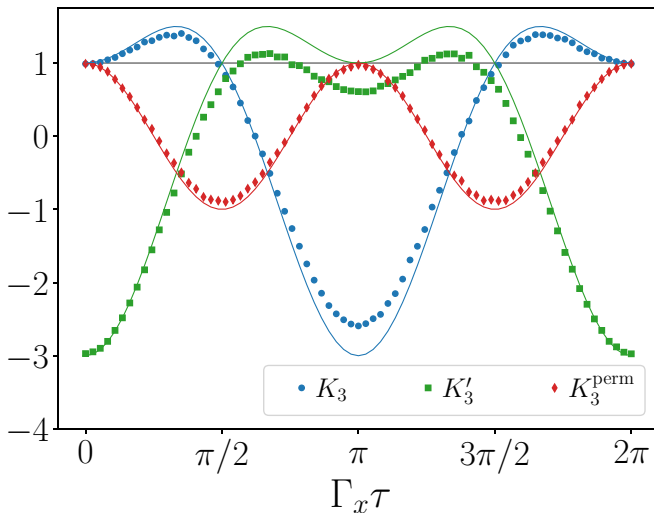


FIG. 5. Same as in Fig. 1 without error mitigation. LGIs as a function of the time difference between two subsequent measurements.

Without the assumption of noninvasive measurability, earlier measurements may affect the following ones and the probabilities do not necessarily come from a joint probability distribution. Considering instead the NIM assumption to hold, measurements do not affect the state of the system or the subsequent system dynamics. Therefore, the order of the measurements is not important; one can drop the subscripts of  $P_{ijk}$  and use the  $P(Q_i, Q_j, Q_k)$  to calculate the three correlation functions:  $C_{12}, C_{23}, C_{13}$ . Starting from the general expression

$$C_{ij} = \sum_{Q_i, Q_j = \pm 1} Q_i Q_j P(Q_i, Q_j) = \langle Q_i Q_j \rangle, \quad (\text{A3})$$

we obtain

dichotomic variable  $Q \rightarrow -Q$  at different times in  $K_3$ . This operation generates the following inequality:

$$-3 \leq K'_3 \leq 1; \quad K'_3 \equiv -C_{12} - C_{23} - C_{13}. \quad (\text{A7})$$

Finally, the last, different, third-order inequality can be obtained from  $K_3$ , just by changing a sign:

$$-3 \leq K_3^{\text{perm}} \leq 1; \quad K_3^{\text{perm}} \equiv -C_{12} + C_{23} + C_{13}. \quad (\text{A8})$$

In principle, one can derive other functions starting from the function  $K_3$  and building all the quantities obtained permuting all the time indices. In our example (three measurements in time, i.e., order 3), the only three different cases are the inequalities proposed above.

## APPENDIX B: ERROR MITIGATION

Quantum error mitigation refers to a series of techniques aimed at reducing (mitigating) the errors that occur in quantum computing algorithms due to hardware limitations. These techniques try to reduce the impact of noise in quantum computations without, in general, completely removing it. As the sources of noise during quantum computing algorithms are present through the whole computation and a complete account of these is a very complex task, we decided to deal only with the error occurring at readout. Namely, we tried to mitigate the readout noise of IBM Quantum, correcting the output of the experiment *a posteriori*. A way to deal with it is already implemented in IBM Quantum and quite simple in its realization; here we give an account of the basics. Let us assume to have an  $n$ -qubit system. We perform a measurement on all the qubits at a certain time and obtain an  $n$ -bit string output. This string could be one of  $2^n$  possible realizations. Now let us assume that the same output is read again and a different outcome is collected. We might imagine that the noise perturbed the measurement outcome, slightly modifying the output string. Easily enough, one could prepare all possible  $2^n$  states of the  $n$ -qubit string and perform a readout on all of them, in the hypothesis that the error on the preparation of



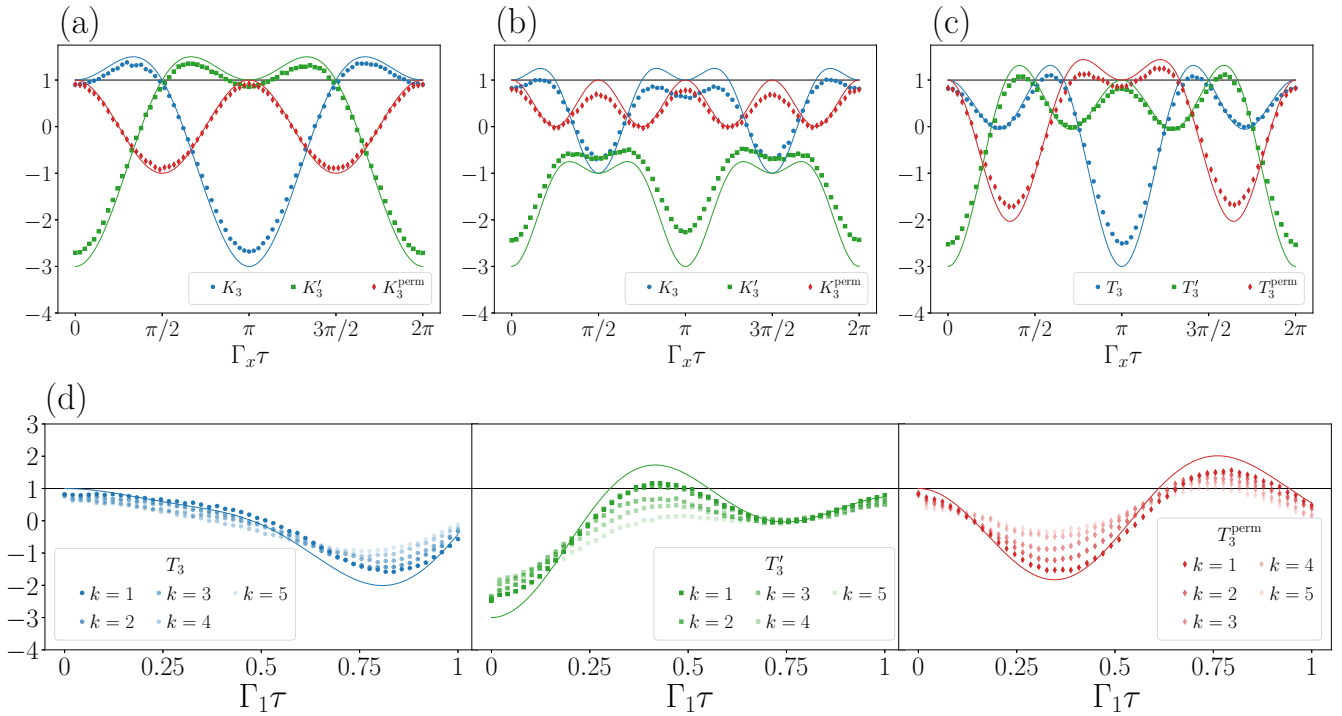


FIG. 6. (a)–(c) As in Fig. 3 without error mitigation; (d) as in Fig. 4 without error mitigation. (a)–(c) LGBIs and LGIs on a two-qubit system. Markers are experimental results; solid lines are numerical predictions obtained with exact diagonalization. (a) LGIs calculated on a single qubit; (b) LGIs considering the total spin of the system; (c) LGBIs; (d) LGBIs calculated for the transverse field Ising chain.

the states is negligible. Repeating the readout several times on each of the  $2^n$  possible states, one can construct a matrix  $M$  which contains the outcome probabilities for each initial state, ideally without errors,  $M = \mathbb{I}$ . In the framework we are working in, we may assume that the noisy measurement output  $\sigma_{\text{noisy}}$  is the product of  $M$  times a noiseless output  $\sigma_{\text{noiseless}}$ :

$$\sigma_{\text{noisy}} = M\sigma_{\text{noiseless}}. \quad (\text{B1})$$

The error mitigated results  $\sigma_{\text{noiseless}}$  are obtained applying  $M^{-1}$  on  $\sigma_{\text{noisy}}$ .

This approach allows one to collect better results than the nonmitigated ones. We also acknowledge that its complexity scales exponentially with the system size, making it necessary to deal with few-qubits measurements. In Fig. 5, we show an explicit example of experimental measurements without error mitigation. The results are a replica of the ones in Fig. 1. When error mitigation is not performed, the performance of the hardware is evidently worse.

For completeness, we also show the results without error mitigation for Figs. 3 and 4 in Fig. 6.

### APPENDIX C: ESTIMATION OF THE PARAMETERS FOR THE INTERACTING EVOLUTION

In this Appendix, we explain the choice of the parameters for the simulation of the many-body system, discussed in Sec. V. We examine the dynamics of  $n$  qubits, initially entangled in a GHZ state  $(|0\rangle^{\otimes n} + |1\rangle^{\otimes n})/\sqrt{2}$ ,

evolving independently according to the Hamiltonian

$$H = \sum_{i=1}^N \frac{\Gamma_i}{2} \sigma_i^x. \quad (\text{C1})$$

In particular in Fig. 7, we show contour plots of  $T_3$ ,  $T_3'$ , and  $T_3^{\text{perm}}$  in two different cases: (i) upper panels show the result of

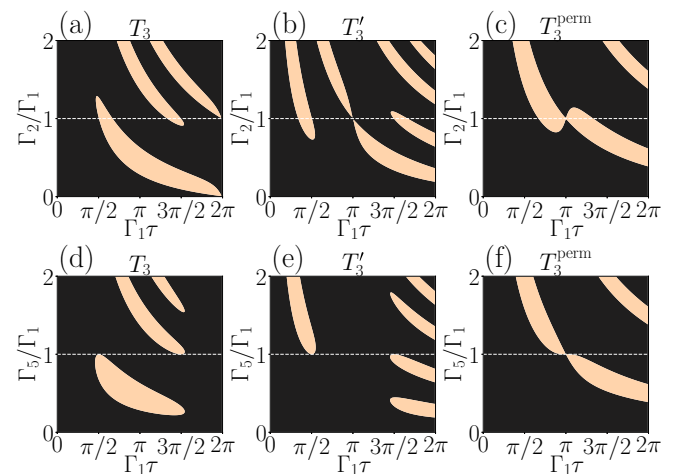


FIG. 7. Contour plot of the LGBIs as a function of time and parameters  $\Gamma_i$  for a system described by Eq. (C1). The results are obtained via exact diagonalization according to Eq. (13). Yellow (black) areas correspond to regions where there is (not) a violation of the LGBIs. Upper panels: simulations for a system of two qubits. Lower panels: simulations for a system of five qubits.

TABLE II. Characterization data of ibmq\_manila quantum device at the time of the experiments.

Quantum hardware properties	Estimated value
Average $\sqrt{X}$ , $X$ , $R_z(\theta)$ error	0.0003
Average CNOT gate error	0.01
Average readout error	0.03
Average relaxation time qubits	140 $\mu\text{s}$
Average decoherence time	60 $\mu\text{s}$
Minimum decoherence or relaxation time	24 $\mu\text{s}$
Gate length	0.03 $\mu\text{s}$

the LGBIs among qubit 1 and qubit 2 for a system composed of two qubits as a function of time and the ratio  $\Gamma_2/\Gamma_1$ ; (ii) lower panels show the same quantities among qubit 1 and qubit 5 evaluated for a system composed of five qubits

as a function of  $\Gamma_5/\Gamma_1$  with  $\Gamma_{2,3,4} = \Gamma_1$ . The black regions correspond to values of the parameters where the LGBIs are not violated; yellow lobes correspond to violations of the inequalities.

We observe that in the case of the two-qubit system, a violation of the inequalities occurs for any value of the ratio  $\Gamma_2/\Gamma_1$  as a function of time. On the other hand, in the case of the five-qubit system for  $\Gamma_5/\Gamma_1 = 1$ , no violation occurs in any of  $T_3$ ,  $T'_3$ , and  $T_3^{\text{perm}}$ . For this reason, in Sec. V, we investigated the case where  $\Gamma_5/\Gamma_1 = 2$  and  $\Gamma_{2,3,4} = \Gamma_1$ .

#### APPENDIX D: HARDWARE PROPERTIES

In this section, we provide experimental details of the quantum device. In Table II, we report the characterization data of the IBM Quantum processor at the time in which the simulations were performed. We refer the reader to the official IBM Quantum site for further details [9].

- [1] J. Preskill, Quantum computing in the NISQ era and beyond, *Quantum* **2**, 79 (2018).
- [2] T. Brydges, A. Elben, P. Jurcevic, B. Vermersch, C. Maier, B. P. Lanyon, P. Zoller, R. Blatt, and C. F. Roos, Probing Rényi entanglement entropy via randomized measurements, *Science* **364**, 260 (2019).
- [3] V. Vitale, A. Elben, R. Kueng, A. Neven, J. Carrasco, B. Kraus, P. Zoller, P. Calabrese, B. Vermersch, and M. Dalmonte, Symmetry-resolved dynamical purification in synthetic quantum matter, [arXiv:2101.07814](https://arxiv.org/abs/2101.07814).
- [4] A. Elben, R. Kueng, H.-Y. R. Huang, R. van Bijnen, C. Kokail, M. Dalmonte, P. Calabrese, B. Kraus, J. Preskill, P. Zoller, and B. Vermersch, Mixed-State Entanglement from Local Randomized Measurements, *Phys. Rev. Lett.* **125**, 200501 (2020).
- [5] A. Neven, J. Carrasco, V. Vitale, C. Kokail, A. Elben, M. Dalmonte, P. Calabrese, P. Zoller, B. Vermersch, R. Kueng *et al.*, Symmetry-resolved entanglement detection using partial transpose moments, *npj Quantum Inf.* **7**, 152 (2021).
- [6] X.-D. Yu, S. Imai, and O. Gühne, Optimal Entanglement Certification from Moments of the Partial Transpose, *Phys. Rev. Lett.* **127**, 060504 (2021).
- [7] A. J. Leggett and A. Garg, Quantum Mechanics versus Macroscopic Realism: Is the Flux there When Nobody Looks? *Phys. Rev. Lett.* **54**, 857 (1985).
- [8] A. J. Leggett, Testing the limits of quantum mechanics: Motivation, state of play, prospects, *J. Phys.: Condens. Matter* **14**, R415 (2002).
- [9] IBM-Quantum, Real quantum computers. Right at your fingertips, <https://quantum-computing.ibm.com/>.
- [10] A. Palacios-Laloy, F. Mallet, F. Nguyen, P. Bertet, D. Vion, D. Esteve, and A. N. Korotkov, Experimental violation of a Bell's inequality in time with weak measurement, *Nat. Phys.* **6**, 442 (2010).
- [11] G. C. Knee, S. Simmons, E. M. Gauger, J. J. Morton, H. Riemann, N. V. Abrosimov, P. Becker, H.-J. Pohl, K. M. Itoh, M. L. Thewalt *et al.*, Violation of a Leggett-Garg inequality with ideal non-invasive measurements, *Nat. Commun.* **3**, 606 (2012).
- [12] J.-S. Xu, C.-F. Li, X.-B. Zou, and G.-C. Guo, Experimental violation of the Leggett-Garg inequality under decoherence, *Sci. Rep.* **1**, 1 (2011).
- [13] M. Goggin, M. Almeida, M. Barbieri, B. Lanyon, J. O'Brien, A. White, and G. Pryde, Violation of the Leggett-Garg inequality with weak measurements of photons, *Proc. Natl. Acad. Sci. USA* **108**, 1256 (2011).
- [14] J. P. Groen, D. Risté, L. Tornberg, J. Cramer, P. C. de Groot, T. Picot, G. Johansson, and L. DiCarlo, Partial-Measurement Backaction and Nonclassical Weak Values in a Superconducting Circuit, *Phys. Rev. Lett.* **111**, 090506 (2013).
- [15] C. Emary, J. P. Cotter, and M. Arndt, Testing macroscopic realism through high-mass interferometry, *Phys. Rev. A* **90**, 042114 (2014).
- [16] C. Budroni, G. Vitagliano, G. Colangelo, R. J. Sewell, O. Gühne, G. Tóth, and M. W. Mitchell, Quantum Nondemolition Measurement Enables Macroscopic Leggett-Garg Tests, *Phys. Rev. Lett.* **115**, 200403 (2015).
- [17] H. Katiyar, A. Brodutch, D. Lu, and R. Laflamme, Experimental violation of the Leggett-Garg inequality in a three-level system, *New J. Phys.* **19**, 023033 (2017).
- [18] K. Wang, C. Emary, X. Zhan, Z. Bian, J. Li, and P. Xue, Enhanced violations of Leggett-Garg inequalities in an experimental three-level system, *Opt. Express* **25**, 31462 (2017).
- [19] S. Bose, D. Home, and S. Mal, Nonclassicality of the Harmonic-Oscillator Coherent State Persisting up to the Macroscopic Domain, *Phys. Rev. Lett.* **120**, 210402 (2018).
- [20] A. Friedenberger and E. Lutz, Assessing the quantumness of a damped two-level system, *Phys. Rev. A* **95**, 022101 (2017).
- [21] V. Vitale, G. De Filippis, A. De Candia, A. Tagliacozzo, V. Cataudella, and P. Lucignano, Assessing the quantumness of the annealing dynamics via Leggett-Garg's inequalities: A weak measurement approach, *Sci. Rep.* **9**, 1 (2019).
- [22] E. Huffman and A. Mizel, Violation of noninvasive macrorealism by a superconducting qubit: Implementation of a Leggett-Garg test that addresses the clumsiness loophole, *Phys. Rev. A* **95**, 032131 (2017).
- [23] H.-Y. Ku, N. Lambert, F.-J. Chan, C. Emary, Y.-N. Chen, and F. Nori, Experimental test of non-macrorealistic cat states in the cloud, *npj Quantum Inf.* **6**, 1 (2020).
- [24] A. Solfanelli, A. Santini, and M. Campisi, Experimental verification of fluctuation relations with a quantum computer, *PRX Quantum* **2**, 030353 (2021).

- [25] F. Tacchino, A. Chiesa, S. Carretta, and D. Gerace, Quantum computers as universal quantum simulators: State-of-the-art and perspectives, *Adv. Quantum Technol.* **3**, 1900052 (2020).
- [26] S. J. Devitt, Performing quantum computing experiments in the cloud, *Phys. Rev. A* **94**, 032329 (2016).
- [27] S. Bravyi, S. Sheldon, A. Kandala, D. C. McKay, and J. M. Gambetta, Mitigating measurement errors in multiqubit experiments, *Phys. Rev. A* **103**, 042605 (2021).
- [28] P. Jurcevic, A. Javadi-Abhari, L. S. Bishop, I. Lauer, D. F. Bogorin, M. Brink, L. Capelluto, O. Günlük, T. Itoko, N. Kanazawa, A. Kandala, G. A. Keefe, K. Krsulich, W. Landers, E. P. Lewandowski, D. T. McClure, G. Nannicini, A. Narasgond, H. M. Nayfeh, E. Pritchett *et al.*, Demonstration of quantum volume 64 on a superconducting quantum computing system, *Quantum Sci. Technol.* **6**, 025020 (2021).
- [29] A. Eddins, M. Motta, T. P. Gujarati, S. Bravyi, A. Mezzacapo, C. Hadfield, and S. Sheldon, Doubling the size of quantum simulators by entanglement forging, *PRX Quantum* **3**, 010309 (2022).
- [30] D. Alsina and J. I. Latorre, Experimental test of mermin inequalities on a five-qubit quantum computer, *Phys. Rev. A* **94**, 012314 (2016).
- [31] G. J. Mooney, C. D. Hill, and L. C. Hollenberg, Entanglement in a 20-qubit superconducting quantum computer, *Sci. Rep.* **9**, 1 (2019).
- [32] Y. Wang, Y. Li, Z.-q. Yin, and B. Zeng, 16-qubit IBM universal quantum computer can be fully entangled, *npj Quantum Inf.* **4**, 1 (2018).
- [33] M. M. Wilde and A. Mizel, Addressing the clumsiness loophole in a Leggett-Garg test of macrorealism, *Found. Phys.* **42**, 256 (2012).
- [34] N. Brunner, D. Cavalcanti, S. Pironio, V. Scarani, and S. Wehner, Bell nonlocality, *Rev. Mod. Phys.* **86**, 419 (2014).
- [35] G. Benenti, G. Casati, D. Rossini, and G. Strini, *Principles of Quantum Computation and Information: A Comprehensive Textbook* (World Scientific, Singapore, 2018).
- [36] J. Dressel and A. N. Korotkov, Avoiding loopholes with hybrid Bell-Leggett-Garg inequalities, *Phys. Rev. A* **89**, 012125 (2014).
- [37] T. C. White, J. Mutus, J. Dressel, J. Kelly, R. Barends, E. Jeffrey, D. Sank, A. Megrant, B. Campbell, Y. Chen *et al.*, Preserving entanglement during weak measurement demonstrated with a violation of the Bell-Leggett-Garg inequality, *npj Quantum Inf.* **2**, 1 (2016).
- [38] M. Thenabadu, G.-L. Cheng, T. L. H. Pham, L. V. Drummond, L. Rosales-Zárate, and M. D. Reid, Testing macroscopic local realism using local nonlinear dynamics and time settings, *Phys. Rev. A* **102**, 022202 (2020).
- [39] M. Thenabadu and M. D. Reid, Bipartite Leggett-Garg and macroscopic Bell inequality violations using cat states: Distinguishing weak and deterministic macroscopic realism, [arXiv:2012.14997](https://arxiv.org/abs/2012.14997).
- [40] E. H. Lieb and D. W. Robinson, The finite group velocity of quantum spin systems, *Commun. Math. Phys.* **28**, 251 (1972).
- [41] C. Emary, N. Lambert, and F. Nori, Leggett-Garg inequalities, *Rep. Prog. Phys.* **77**, 016001 (2013).
- [42] S.-S. Majidy, H. Katiyar, G. Anikeeva, J. Halliwell, and R. Laflamme, Exploration of an augmented set of Leggett-Garg inequalities using a noninvasive continuous-in-time velocity measurement, *Phys. Rev. A* **100**, 042325 (2019).
- [43] S. Majidy, J. J. Halliwell, and R. Laflamme, Detecting violations of macrorealism when the original Leggett-Garg inequalities are satisfied, *Phys. Rev. A* **103**, 062212 (2021).
- [44] C. Budroni and C. Emary, Temporal Quantum Correlations and Leggett-Garg Inequalities in Multilevel Systems, *Phys. Rev. Lett.* **113**, 050401 (2014).
- [45] N. Lambert, K. Debnath, A. F. Kockum, G. C. Knee, W. J. Munro, and F. Nori, Leggett-Garg inequality violations with a large ensemble of qubits, *Phys. Rev. A* **94**, 012105 (2016).
- [46] T. Fritz, Quantum correlations in the temporal Clauser-Horne-Shimony-Holt (CHSH) scenario, *New J. Phys.* **12**, 083055 (2010).
- [47] S. F. Huelga, T. W. Marshall, and E. Santos, Proposed test for realist theories using Rydberg atoms coupled to a high- $q$  resonator, *Phys. Rev. A* **52**, R2497 (1995).
- [48] A. Cervera-Lierta, Exact Ising model simulation on a quantum computer, *Quantum* **2**, 114 (2018).
- [49] A. Smith, M. Kim, F. Pollmann, and J. Knolle, Simulating quantum many-body dynamics on a current digital quantum computer, *npj Quantum Inf.* **5**, 1 (2019).